Review Article | Technology, Experiment, and Physics

eISSN 2005-8330
https://doi.org/10.3348/kjr.2020.0996
Korean J Radiol 2021;22(6):970-982

Korean Journal of Radiology
KJR

Clinical Applications of Dual-Energy CT

Saira Hamid[1], Muhammad Umer Nasir[2], Aaron So[3], Gordon Andrews[1], Savvas Nicolaou[2], Sadia Raheez Qamar[4]

[1]Department of Radiology, University of British Columbia Hospital, University of British Columbia, Vancouver, Canada; [2]Department of Medical Imaging, Vancouver General Hospital, University of British Columbia, Vancouver, Canada; [3]Department of Medical Biophyics, Schulich School of Medicine and Dentistry Western University London, Ontario, Canada; [4]Department of Medical Imaging, Sunnybrook Hospital, University of Toronto, Toronto, Canada

Dual-energy CT (DECT) provides insights into the material properties of tissues and can differentiate between tissues with similar attenuation on conventional single-energy imaging. In the conventional CT scanner, differences in the X-ray attenuation between adjacent structures are dependent on the atomic number of the materials involved, whereas in DECT, the difference in the attenuation is dependent on both the atomic number and electron density. The basic principle of DECT is to obtain two datasets with different X-ray energy levels from the same anatomic region and material decomposition based on attenuation differences at different energy levels. In this article, we discuss the clinical applications of DECT and its potential robust improvements in performance and postprocessing capabilities.

Keywords: *DECT; Metal artifacts; COVID-19; Acute hemorrhage*

INTRODUCTION

Dual-energy computed tomography (DECT) has emerged as a promising tool in diagnostic imaging with multiple potential clinical applications. It allows identification of the material composition by gathering tissue characterization information based on two absorption measurements at different photon spectra with high and low-energy levels [1]. Based on this differential tissue attenuation, DECT can quantify the iodine content, which helps to identify visceral enhancements, such as hypo- or hyperenhancement, in cases of inflammation. Virtual nonenhanced images can be generated using this dual-energy technique, which can lower the radiation dose exposed by a patient by eliminating the need to perform a non-contrast phase. In venous phase abdominal imaging, areas of hyperdensity could either represent a hematoma or true enhancement of the lesion; moreover, the presence of calcifications can pose a diagnostic challenge to be certain about its differentiation from a hemorrhage. Furthermore, the ability of dual-energy CT to substantially reduce metallic prosthesis-related artifacts is an added advantage that can reveal the underlying anatomical and pathological details.

Iodine images can be displayed as quantitative gray-scale images or color overlay maps, both of which improve lesion conspicuity due to differences in the iodine content between lesions and normal parenchyma. Iodine images can detect and quantify iodine within each image voxel, allowing the detection of even a small amount of enhancement within a lesion [1]. To illustrate improved tissue characterization, in this article, liver lesions, renal masses, and renal stone characterization will be briefly discussed. The role of DECT in oncologic imaging will also be outlined.

Received: September 14, 2020 **Revised:** November 16, 2020
Accepted: November 22, 2020
Corresponding author: Saira Hamid, MBBS, FCPS, Department of Radiology, University of British Columbia Hospital, University of British Columbia, Koerner Pavilion, 2211 Wesbrook Mall UBC Hospital, Vancouver, BC V6T 2B5, Canada.
• E-mail: saira.hamid@vch.ca

Techniques

At present, there are five approaches to DECT: sequential acquisition, rapid voltage switching, DSCT, layer detectors, and energy-resolving or quantum-counting detectors;

Korean Journal of Radiology
KJR

currently, only the former three are commercially available.

In DECT, information can be gathered through two absorption measurements as two-photon spectra. It can differentiate between tissues and other materials by utilizing the property of X-ray attenuation change at different photon spectra.

Careful attention should be given while protocolling patients with an acute abdomen. For instance, when there is clinical suspicion of urolithiasis or suspected non-traumatic hemorrhage, generally, no intravenous (IV) contrast is administered for initial CT evaluation. IV contrast is generally administered to patients with a Glomerular filtration rate > 30. In our department, an appropriate weight amount of iodinated contrast at an infusion rate of 2–3 mL/s is administered through a peripheral IV catheter; thereafter, venous phase images are acquired from the dome of the diaphragm to the inferior aspect of the symphysis pubis.

In the venous phase images, areas of hyperdensity could represent hemorrhage or enhancement of the lesion. Furthermore, the presence of calcifications makes it even more difficult to determine hemorrhage. DECT images alongside virtual non-contrast (VNC) images can help to subtract contrast to differentiate between enhancement and hemorrhage. The visual difference in the foci of mineralization at different energy levels helps to differentiate calcified areas from hemorrhage.

Administration of oral contrast is dependent on personal preference, complexity of the case, and the patient's body type. It helps to better delineate various bowel pathologies; for example, the appendix with intraluminal contrast and enteric fistula are easier to evaluate. However, oral contrast can mask gastrointestinal bleed and is contraindicated in high-grade small bowel obstruction or possible ischemia. Moreover, oral contrast delays the examination and increases patients' length of hospital stay.

Material Separation

Blended images are generated through a combination of the acquired low-energy (80 kilovoltage peak [kVp]) and high-energy (140 kVp) datasets to simulate a standard 120-kVp dataset. Virtual monoenergetic images were acquired to simulate a scan obtained at a single-energy level. Virtual monochromatic (VMC) images can be manually changed to a specific energy level for various clinical applications. Artifacts from metal implants can be reduced using a high-energy monoenergetic beam (95–140 kiloelectron volt [keV]). Intermediate-energy virtual monoenergetic images (60–75 keV) are ideal for evaluation of soft tissues due to the balance between adequate contrast and reduced image noise. Lesions with an inherently high contrast can be best evaluated using a low-energy monoenergetic beam (45–55 keV) [1].

DECT utilizes a three-material decomposition algorithm to create soft tissue-, fat-, and iodine-material-specific images. Contrast-enhanced images are more accurate measures of enhancement as they show the amount of iodine distribution in the tissues and are independent of inherent tissue attenuation. For example, in liver masses, iodine quantification can be used to accurately measure actual tumor enhancement without adding liver parenchymal enhancement. Virtual unenhanced DECT images can be obtained and are comparable to unenhanced images.

Tissue Characterization

Dual-energy applications add value to CT imaging due to superior lesion detection and characterization. The single most important property that governs the interpreter's ability to detect a lesion in the background of normal tissue is the contrast-to-noise ratio (CNR).

Intermediate intensity monoenergetic beams (60–75 keV) eliminate very low-energy photons that contribute only to image noise and, therefore, improve the overall image quality [2,3].

Utilization of DECT in Head and Neck Imaging

Head and Neck Oncology

DECT can be useful in differentiating malignancies from other conditions, such as hemorrhagic brain metastasis from intracranial hemorrhage. Using a monoenergetic beam of 40 keV improves tumor delineation. Moreover, DECT can differentiate hyperdense hemorrhage from enhancement within a hemorrhagic mass. It has been suggested that 65-keV VM images provide the best overall image quality, and that 40-keV VM images enable the best tumor delineation [4].

Brain Trauma

DECT can distinguish contrast and hemorrhage based on the different spectral ranges of blood and iodine. DECT also allows the extraction of a virtual unenhanced scan from a contrast-enhanced scan. Moreover, DECT helps to differentiate hyperdensity secondary to intracranial hemorrhage from iodine extravasation or staining (Fig. 1), especially in stroke patients undergoing a hemorrhagic

 https://doi.org/10.3348/kjr.2020.0996

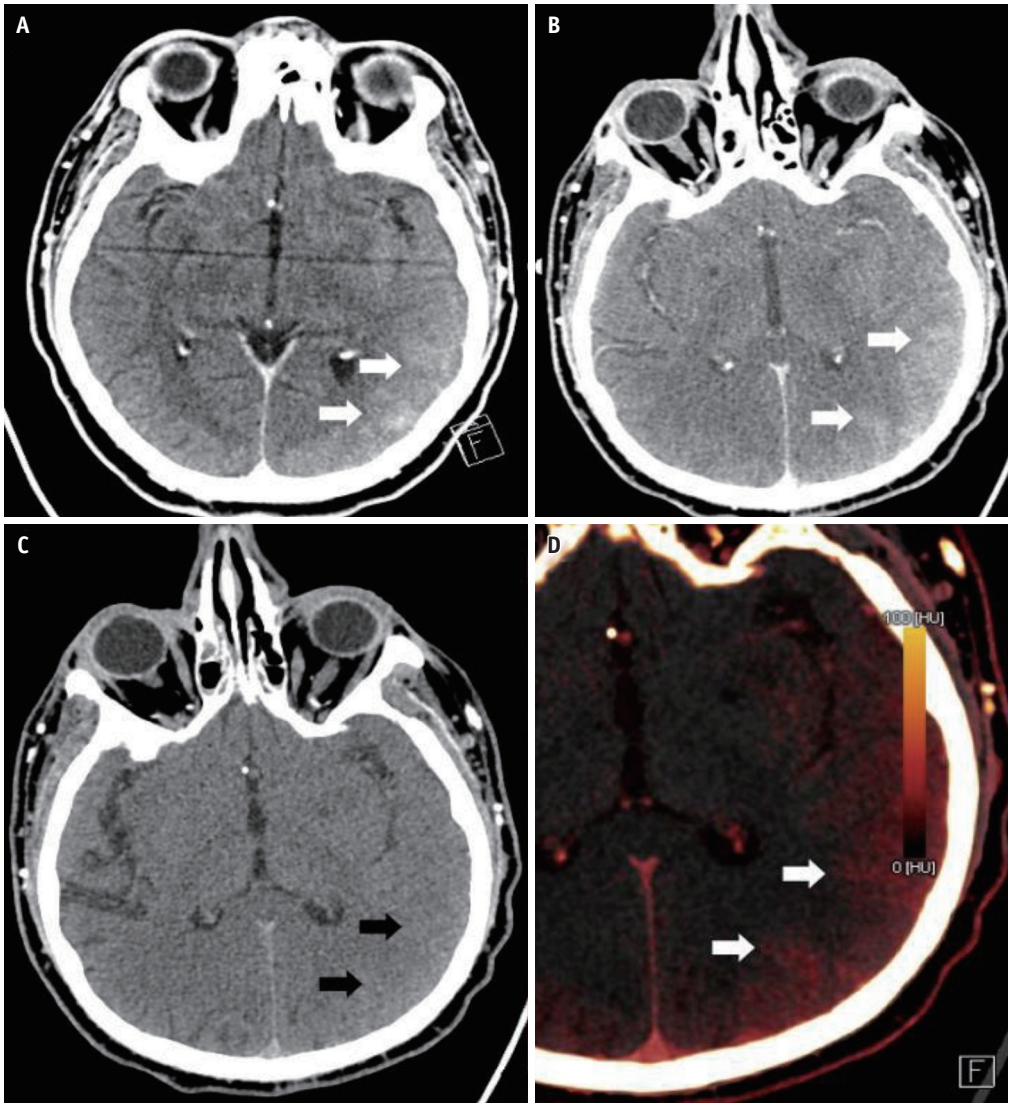

Fig. 1. A 48-year-old male with post-tissue plasminogen activator after left middle cerebral artery infarct.
A. Axial CT head image shows evolving left MCA infarction displaying local mass effect with sulcal effacement in the left temporal and parieto-occipital lobes. High attenuation gyri (arrows) in this region can either be due to petechial hemorrhage or contrast staining. Dual-energy CT head. **B.** Post-contrast image demonstrates contrast staining in the region of infarction seen as hyperattenuating gyri (arrows). **C.** Virtual non-contrast image corresponding to normal gyri appearance (arrows) and no corresponding high-density areas, confirming contrast staining rather than hemorrhage. **D.** Color coded iodine map shows the distribution of iodine in the regions of contrast staining (arrows).

transformation after intraarterial recanalization.

Studies suggest that the virtual monoenergetic images acquired at 190 keV can better differentiate enhancing subdural effusions from subdural hemorrhage [5,6]. In the assessment of brain parenchyma on non-contrast CT, improved image quality was demonstrated with VM imaging at 65–75 keV when compared to a single-energy CT [7,8].

Utilization of DECT in Cardiothoracic Imaging

Thoracic Oncology

For thoracic oncologic CT applications, studies suggest that subjective image quality for visualization of lung carcinoma is improved at 55–70 keV [9,10] compared with conventional CT scans. In thoracic oncology, DECT can be used to differentiate benign and malignant pulmonary nodules and masses [11]. Moreover, DECT can be used for cases of anterior mediastinal lesions to differentiate thymic cysts from thymic epithelial tumors [11].

Cardiac Evaluation

Efficient detection of myocardial infarction by DECT, in addition to evaluation of coronary arteries, has prognostic implications [12,13]. DECT depicts myocardial perfusion

https://doi.org/10.3348/kjr.2020.0996

Korean Journal of Radiology
KJR

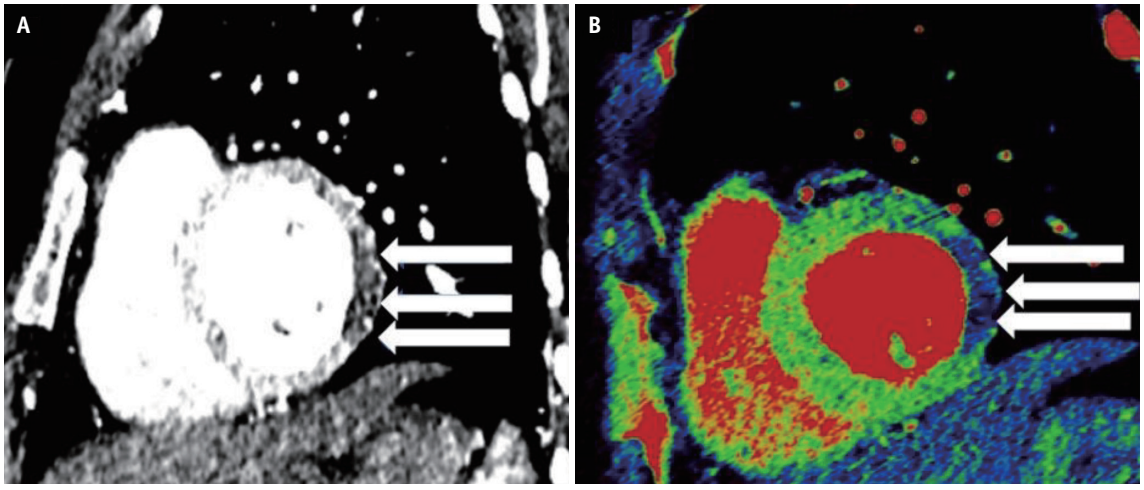

Fig. 2. A 68-year-old male presented to the emergency department with acute chest pain.
A, B. CT chest sagittal image **(A)** shows hypoattenuating myocardium, which corresponds to a decreased iodine uptake in the left ventricular free wall suggesting perfusion defect (arrows) depicted as blue color, coded on **(B)** iodine overlay images (arrows).

defects (Fig. 2) more conspicuously than conventional CT scanning [14].

Different studies have demonstrated that using low virtual monoenergetic keV improves the visualization of myocardial fibrosis. For instance, in an animal study, there was an improved detection of chronic infarct with 40-keV VM images compared with single-energy CT scans [15]. Furthermore, a subsequent study [16] demonstrated that compared with MRI, use of a 70 keV virtual monoenergetic beam can identify myocardial late enhancement and pattern classification (subendocardial, epicardial, transmural, meso-myocardial, and/or patchy).

COVID-19 Pneumonia

Dual-energy CT imaging can provide added information about any pulmonary pathology by highlighting the perfusion abnormalities associated with the disease. CT findings of Coronavirus disease-19 (COVID-19) pneumonia include ground-glass opacification, consolidation, atoll sign (or "reverse halo" sign), halo sign, organizing pneumonia, and vascular dilatation adjacent to the pulmonary pathology, commonly seen as a later manifestation of the disease. Perfusion analysis of the pulmonary parenchyma in COVID-19 shows features of high iodine density or increased perfusion of the lung parenchyma around the pulmonary opacity, which is likely secondary to vascular dilation contributing to a higher volume of blood flow. The etiology of vascular dilatation can be attributed to the inflammatory cascade or microvascular thrombosis. The areas of pulmonary opacity showed reduced perfusion on dual-energy maps (Fig. 3) [17].

Utilization of DECT in Abdominal Imaging

Abdominal Oncology

Several studies have demonstrated that the conspicuity of hyperattenuating and hypervascular liver lesions is greater at low keV than with conventional CT scanners [18-20]. It was also documented that an increase in noise with a low KeV monoenergetic beam in patients with increased body size can decrease the contrast noise ratio [17]. Various optimal energy settings have been described depending on the body size for optimized visualization of hypervascular liver lesions [21].

In patients with pancreatic adenocarcinoma, 55-keV VM images have been found to improve visualization of tumors and vascular infiltration [22] when compared with linearly blended reconstructions; however, 70 keV represented the best subjective overall energy level [23].

For VM CT of renal cell carcinoma, tumor delineation was optimal at 40 keV [24]. A level of 50 keV appears to be the optimal overall compromise between the keV settings for the routine reconstruction of high-contrast VM images. Other studies aimed to determine the optimal thresholds for the differentiation between vascular and nonvascular renal lesions, with the recommended energy levels of 40–60 keV [25].

An iodine concentration of 2.0 mg/mL represented the optimal threshold to discriminate between lymphoma and lymph node metastasis (sensitivity, 87%; specificity,

 https://doi.org/10.3348/kjr.2020.0996

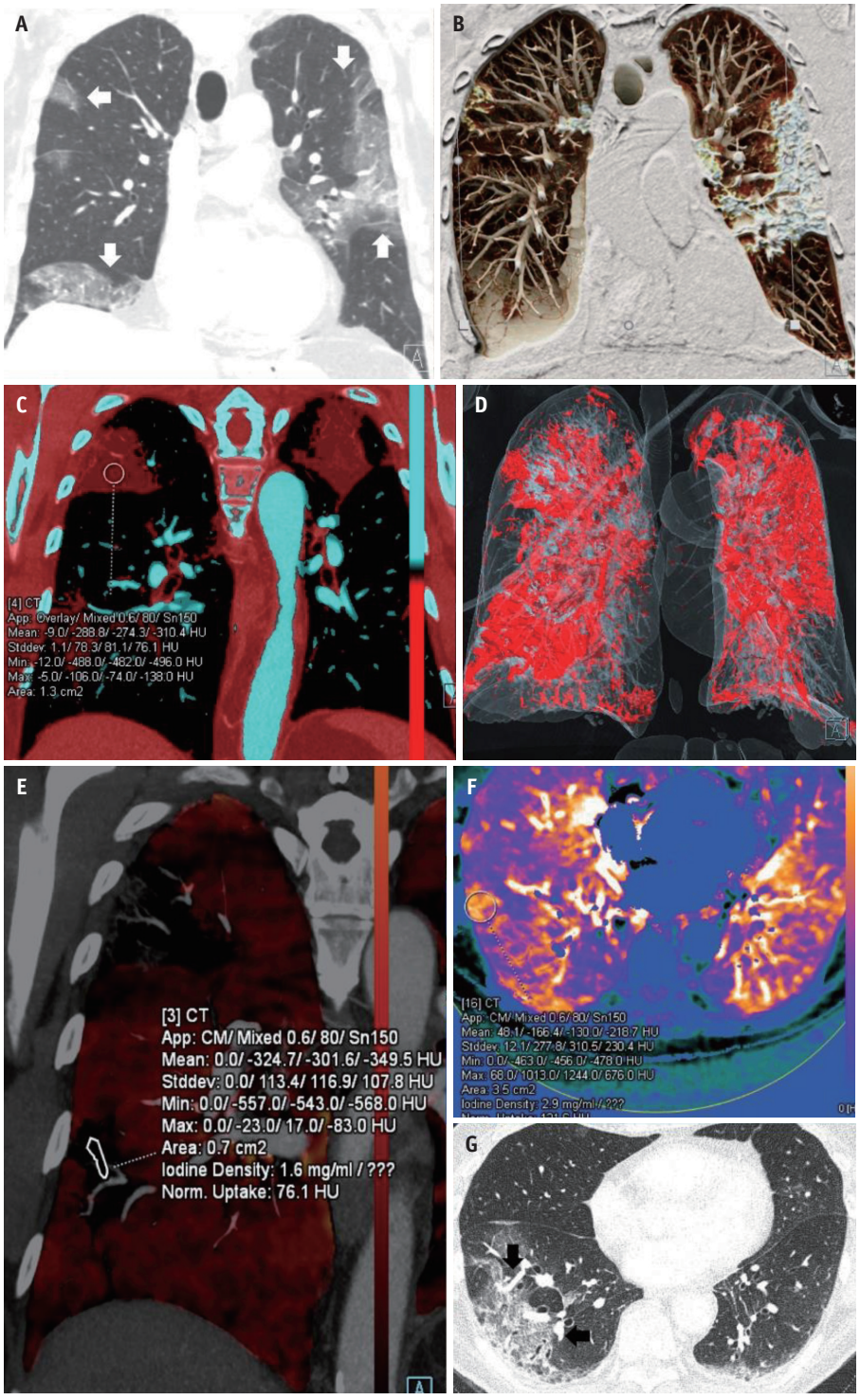

Fig. 3. 76-years-old male with polymerase chain reaction-positive COVID-19 pneumonia.
A. CT chest coronal reformatted image with lung window shows multifocal predominantly peripherally distributed areas of consolidation in both lungs (arrows). **B.** Coronal clip plane cinematic rendered CT chest image displays similar pattern of the pulmonary involvement with dense consolidation. **C.** Color coded iodine map with red color highlighting consolidation quantifying the iodine content. **D.** Volume rendered three-dimensional image analysis reveals the snapshot of total lung volume involvement. **E.** Dual-energy CT chest with color coded iodine overlay maps displaying peripheral areas of consolidation in the right upper and lower lobe with reduced iodine uptake measured at 1.6 mg/mL. **F.** Dual-energy CT analysis (dense lung protocol) post processed on Siemens Syngo.via (VB30) shows the areas of increases perfusion around the relatively hypoperfused pulmonary consolidation. **G.** Axial CT image (lung windows) shows right greater than left lower lobe multifocal bronchial wall thickening and peripheral areas of ground-glass, consolidation and septal thickening with organizing pneumonia pattern. Peripheral dilatation of vessels (arrows) on the lung windows presumably represent pre-stenotic dilation.

https://doi.org/10.3348/kjr.2020.0996

Korean Journal of Radiology
KJR

89%) [26].

Bowel Evaluation

In patients with small bowel obstruction, mural enhancement of the bowel can be detected with increased diagnostic confidence in 70-keV VM images [27]. Recent studies have shown that iodine overlay imaging and virtual monoenergetic imaging at lower energy levels (40-keV) can detect and differentiate mural hypoperfused segments from the normally perfused bowel wall [28]. Furthermore, the 40-keV VM imaging has added diagnostic value in the evaluation of inflammatory intestinal lesions in Crohn's disease owing to greater conspicuity [29].

DECT can detect a change in bowel wall enhancement and thus is extremely helpful in suspected bowel injury. Iodine map images can increase the visibility of the iodine content in bowel wall and VNC images, thus increasing the diagnostic confidence of visualizing intramural hemorrhage [30].

Gangrenous Appendicitis and Cholecystitis

Long-standing, progressive transmural inflammation causes ischemia and necrosis of the appendix, thus resulting in gangrenous appendicitis, which is prone to complications such as perforation, abscess formation, and sepsis. It is important to identify gangrenous appendicitis preoperatively, as the rate of postoperative complications is relatively higher than that of uncomplicated appendicitis. Dual-energy CT can detect the presence of transmural necrosis of the appendix wall on the iodine overlay images and low 40-keV virtual monoenergetic images. The ability of the dual-energy CT to distinctly differentiate gangrenous mucosa from the normal enhancing mucosa clearly adds value to patient management (Fig. 4) [25].

Dual-energy can demonstrate areas of absent wall enhancement consistent with gangrenous cholecystitis (Fig. 5). Identification of gangrenous cholecystitis has been shown to alter the surgical approach with the need for an open rather than a laparoscopic cholecystectomy.

Gall Stones and Renal Calculi

Dual-energy CT can be extremely helpful in identifying the composition of various gall stones [30]. Previous studies

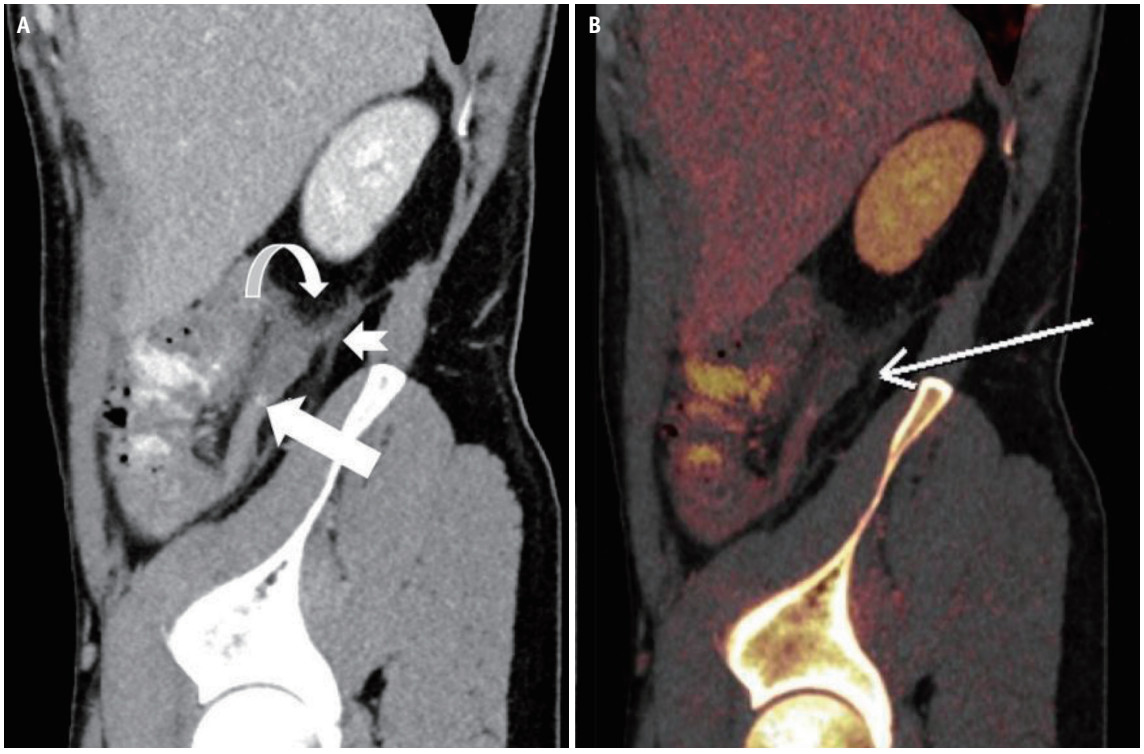

Fig. 4. A 40-year-old male who presented with a 24-hours history of abdominal pain, which was more marked in the right lower quadrant.

A, B. Dual-energy CT **(A)** source sagittal image shows dilated retrocecal appendix with mural thickening, surrounding inflammatory fat stranding (curved arrow), thickening of peritoneal reflections (notched arrow) and trace free fluid consistent with acute appendicitis. A 5-mm hyperdense appendicolith (arrow) in the mid appendix. **(B)** Color coded iodine maps reveals an area of reduced iodine uptake along the posterior wall of the appendicular tip with reduced iodine uptake (arrow), concerning for early gangrenous appendicitis with histopathologic confirmation of acute appendicitis with mural necrosis.

https://doi.org/10.3348/kjr.2020.0996

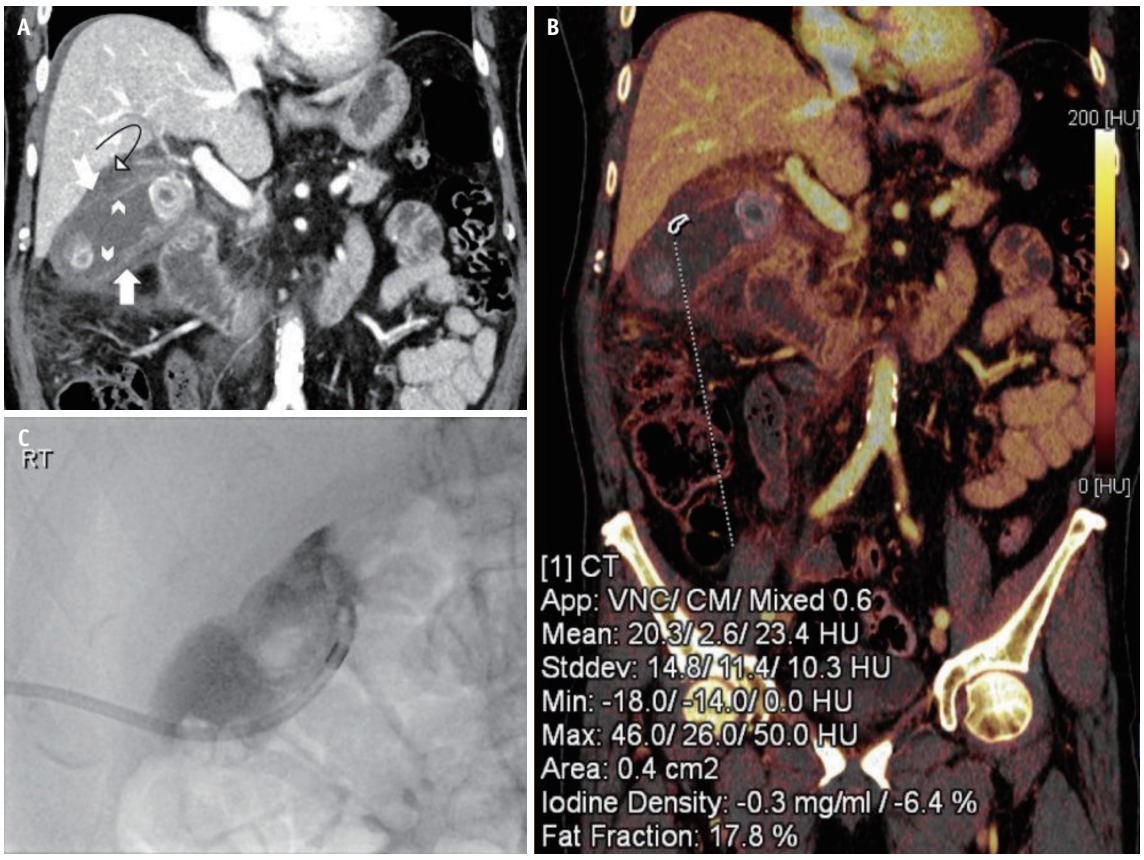

Fig. 5. A 77-years-old male who presented with a 2-day history of abdominal pain and distension with obstipation.
Past medical history revealed treated colon carcinoma. **A.** Distended gallbladder with pericholecystic edema and mural thickening (arrow). Focal areas of the gallbladder wall display decreased enhancement (chevron arrows). Mural defect in the cranial aspect of the gallbladder body (notched arrow) with perforation and incompletely imaged walled off collection (curved arrow) in the gallbladder fossa. **B.** Color coded iodine map reveals the lack of iodine uptake in the region of perforated gallbladder wall suggesting mural necrosis. **C.** Percutaneous cholecystostomy was done to relieve the symptoms.

have shown that gallstones are better visualized on a monochromatic high keV [31]. Dual-energy CT can identify the specific composition of the calculus and differentiate non-uric acid calculi from uric acid calculi [31].

Utilization of DECT in Vascular Imaging

Carotid Artery Evaluation

Studies have demonstrated that virtual monoenergetic imaging at 40–60 keV for dual-energy CT angiography (CTA) provides superior subjective and objective image quality for the evaluation of the carotid and cerebral arteries [32-34]. Blooming artifacts from calcified plaques and accurate assessment of the degree of stenosis in the presence of calcified plaques were reported at 80–100 keV [32]. Furthermore, virtual monoenergetic imaging is helpful in the evaluation of arteries that are close to the skull [14,33,35].

Pulmonary Angiography

Using DECT perfusion scans, perfusion defects beyond obstructive clots can be identified (Fig. 6) [14,36]. Pontana et al. [37] demonstrated that blood flow images can detect subsegmental perfusion defects, whereas endoluminal thrombi cannot be visualized in the corresponding arteries using pulmonary CTA.

One of the most important applications of DECT is to detect small embolic vessel occlusion, and one of the studies highlighted the usefulness of virtual monoenergetic imaging in suboptimal scan secondary to technique or missed timing of contrast bolus [38]. Virtual monoenergetic images at 70 keV for CT pulmonary angiography are recommended by one of the studies [39].

Aorta, Abdomen, and Lower Extremity Angiography

The standard CT arteriography protocol for the assessment of acute aortic syndromes includes unenhanced images

https://doi.org/10.3348/kjr.2020.0996

Korean Journal of Radiology
KJR

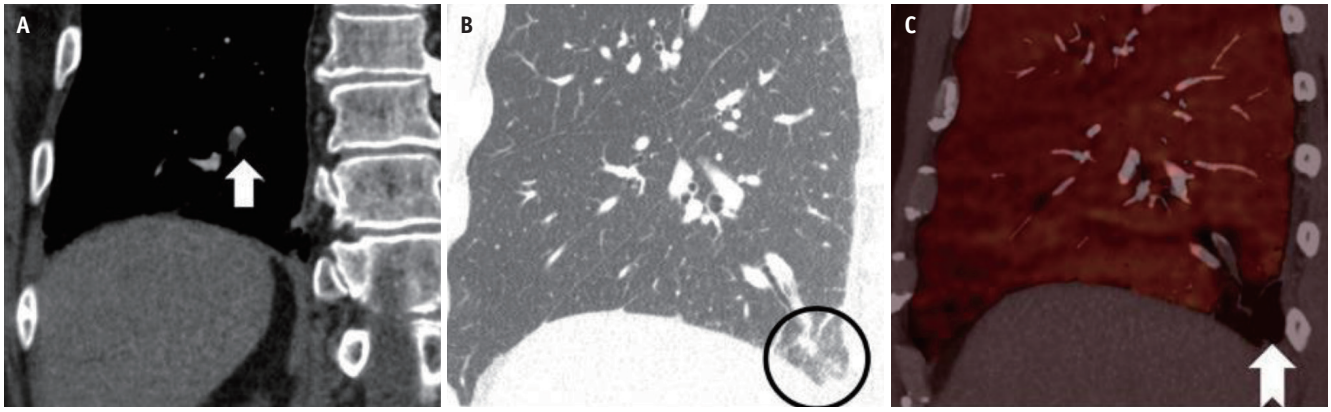

Fig. 6. A 68-year-old male with right pleuritic chest pain and ipsilateral flank area pain.
A, B. CT pulmonary angiogram **(A)** cropped coronal image shows a filling defect (arrow) in the right posterior basal subsegmental branch consistent with pulmonary embolism. **(B)** Sagittal CT chest lung window shows a focal ground-glass (circle) consistent with an evolving infarct in the posterior basal right lower lobe corresponding to an area of decreased perfusion (notched arrow) evident on **(C)** iodine overlay maps.

to detect hyperdense intramural hematoma or intimal calcifications and to detect dissection, which results in considerable radiation exposure. Although virtual unenhanced images are slightly noisier compared with unenhanced images, they are diagnostic in almost 95% of cases [40].

By using the overlay maps, the differences between the high attenuation due to blood, bone, or contrast agent are highlighted, and the diagnostic accuracy for detection of endoleak is increased [41].

The precise removal of calcium from arteries assists in the better evaluation of atherosclerotic arteries [42]. However, this technique is not very helpful for small arteries. The increase in radiation dose, noise, and small diameter of the distal peripheral arteries are limitations for dual-energy peripheral CTA. High-resolution dual-energy acquisitions combined with iterative reconstruction and spectral filtering can be a solution to this problem [43].

Low keV virtual monoenergetic imaging at 60 keV or less has been shown to provide improved CNR and qualitative image quality [44,45]. Virtual monoenergetic imaging at 40 keV has been shown to improve diagnostic accuracy for the detection of acute arterial bleeding [46] and endoleaks [47]. Furthermore, it has been demonstrated that the diagnostic accuracy of CTA for lower extremity run-off for the detection of significant stenosis (50%) can be effectively increased by using 40-keV VM images compared with linearly blended reconstructions (accuracy: 96.4% vs. 89.3%, respectively) [48].

CT Venography or Portal Venous Phase Imaging

Virtual monoenergetic images at 40 keV provide greater contrast attenuation and assessment of poorly opacified liver veins than linearly blended images, such as in cirrhotic livers [49]. Low keV virtual monoenergetic images have also been shown to improve the assessment of the portal vein and deep vein thrombosis [50]. Both iodine maps and VM images at 40 keV provide substantially higher diagnostic confidence and accuracy in detecting and differentiating venous thrombosis from iodine flux artifacts compared with linearly blended dual-energy CT scans [51].

Utilization of DECT in Musculoskeletal Application

Bone Marrow Edema

In older patients with multiple fractures of varying ages and patients with subtle fractures, it can be difficult to assess using conventional CT. Bone marrow edema (BME) is a biomarker of occult fractures, and various studies have shown that DECT material decomposition and virtual non-calcium imaging can detect BME (Supplementary Fig. 1) [52]. In patients with abdominal and pelvic trauma, VNC images can be created to differentiate chronic fractures from acute and non-displaced occult fractures.

Gout

DECT demonstrates great promise for the diagnosis of gout. DECT gout application can be used as an excellent noninvasive alternative to synovial fluid aspiration. Moreover, DECT is increasingly useful in diagnosing cases of gout where synovial fluid fails to demonstrate monosodium urate crystals (Supplementary Fig. 2).

Metal Artifact Reduction

DECT measures attenuation at two different energy

 https://doi.org/10.3348/kjr.2020.0996

levels. Beam-hardening and metallic streak artifacts can be reduced by using high-energy X-ray photons as they penetrate deeper into the materials (Supplementary Fig. 3). Simulated monochromatic images have been shown to decrease the number of artifacts caused by dental hardware in adjacent bones [53]. Subjectively superior images can be obtained by using simulated high-energy reconstructions in the region of metallic hardware [54-56]. A recent cadaveric study showed that increasing the simulated monochromatic energy level of the reconstructed data resulted in subjectively decreased beam-hardening artifacts from dental implants [57]. In another study, DECT with postprocessing for metal artifact reduction software (MARS, GE Healthcare) improved the depiction of blood vessels adjacent to a platinum coil mass in patients with intracranial aneurysm embolization [58].

In comparison with single-energy CT [57] and linearly blended dual-energy CT [53,59], the virtual monoenergetic imaging at 100 keV decreases the streak artifacts from dental implants. Similarly, artifacts from spinal fixators have been demonstrated to reduce at levels greater than 110 keV [60,61], with partially reduced artifacts at these keV settings compared with single-energy CT [55]. In the pelvis, the benefit of VM imaging at 130 keV or greater for artifact reduction in patients with hip prosthesis has been demonstrated in comparison with single-energy CT and linearly blended dual-energy CT [59]. There is accumulating evidence demonstrating the usefulness of dedicated metal artifact reduction algorithms as an addition or alternative to VM imaging. For pelvic CT in patients with hip implants, VM images at 200 keV were preferred for bone assessment, whereas a dedicated metal artifact reduction algorithm was considered superior for analyzing soft tissue [62]. Metal artifact reconstruction algorithms were found to be more effective than VM imaging in artifacts arising from deep brain stimulating electrodes [63]. Combining metal artifact reduction software with high keV VM imaging has also been suggested to achieve the greatest artifact reduction in patients with orthopedic foreign bodies in the spine [63].

Image Quality and Radiation Dose Considerations

Several studies have shown significant dose reductions or similar doses when compared to single-energy CT exams [64,65]. Current efforts in radiology to minimize patient radiation exposure preclude the wide implementation of techniques that would increase patient dose [64]. One study demonstrated that DECT imaging at 80 and 140 kVp and simulating a 120-kVp single-source image results in a dose-length product and CT dose index values of 10 and 12% less than standard single-energy CT acquisitions, with no significant difference in objective image noise or subjective image quality [65].

Several investigations have shown that the iodine load for abdominal CTA can be reduced by up to 50% with the

Table 1. Dual-Energy CT Applications Summary

Location/Region	Material Seperation/Virtual Monoenergetic Beam	Iodone Quantification
Brain	Helps to differentiate between tumor and bleed	Helps to differentiate between bleed and contrast
Cardiac	Low virtual monoenergetic KeV improves visualization of myocardial fibrosis	
Lungs		High iodine density/increased perfusion of the lung parenchyma around the pulmonary opacity in COVID-19 Decrease perfusion of the lung parenchyma in the region of pulmonary infarct suggesting hypoperfused lung/pulmonary embolism
Abdomen	Differentiate mural hypoperfused segment from normal perfused bowel wall Differentiate tumors Helpful in identifying the composition of various kidney/gall stones	Iodine map images can increase the visibility of the iodine content in bowel wall and thus increasing the diagnostic confidence of visualizing intramural hemorrhage
Vascular imaging	Blooming artifacts from calcified plaques can be reduced	
Bones	VNC images can be created to differentiate chronic fractures from acute and non-displaced CT occult fractures	
Metallic artifacts	High monoenergetic beam can reduce metallic artifacts	

keV = kiloelectron volt, VNC = virtual non-contrast

https://doi.org/10.3348/kjr.2020.0996

Korean Journal of Radiology
KJR

use of VM reconstructions at 40–60 keV (reduction in iodine dose: -49% [63,66], -27% [67], and -28% [68], compared with single-energy CT while providing equivalent or improved CNR as well as superior subjective vascular contrast attenuation.

Limitations

The limitations of DECT include higher image noise on virtual unenhanced images than unenhanced images, consumes more time and expertise to process and generate images, larger image datasets requiring increased storage capabilities, and the inability to quantify attenuation in Hounsfield units on virtual unenhanced images obtained with current processing techniques. This last drawback might eventually be overcome by modified image-processing algorithms, allowing the extrapolation of attenuation data.

CONCLUSION

DECT, with its unique abilities, has a multitude of clinically applicable advantages as compared to the conventional single-energy CT scan. Thus, helping create a paradigm shift in the modern advancing field of medical imaging (Table 1).

Supplement

The Supplement is available with this article at https://doi.org/10.3348/kjr.2020.0996.

Conflicts of Interest

The authors have no potential conflicts of interest to disclose.

Author Contributions

Conceptualization: Savvas Nicolaou, Sadia Raheez Qamar, Aoron So. Data curation: Saira Hamid, Muhammad Umer Nasir. Formal analysis: Saira Hamid. Investigation: Saira Hamid, Muhammad Umer Nasir, Gordon Andrews. Methodology: Saira Hamid. Project administration: Sadia Raheez Qamar, Savvas Nicoloau, Saira Hamid. Resources: Savvas Nicoloau, Gordon Andrews. Software: Muhammad Umer Nasir. Supervision: Sadia Raheez Qamar, Savvas Nicoloau. Validation: Saira Hamid, Savvas Nicolaou. Visualization: Saira Hamid, Savvas Nicolaou, Sadia Raheez Qamar. Writing—original draft: Saira Hamid. Writing—review & editing: Saira Hamid, Muhammd Umer Nasir, Aoron So.

ORCID iDs

Saira Hamid
https://orcid.org/0000-0001-6130-9368
Muhammad Umer Nasir
https://orcid.org/0000-0003-0935-3227
Aaron So
https://orcid.org/0000-0001-9293-158X
Gordon Andrews
https://orcid.org/0000-0002-2329-3489
Savvas Nicolaou
https://orcid.org/0000-0002-4203-6605
Sadia Raheez Qamar
https://orcid.org/0000-0001-6637-6092

REFERENCES

1. Grajo JR, Patino M, Prochowski A, Sahani DV. Dual energy CT in practice: basic principles and applications. *Appl Radiol* 2016;45:6-12
2. Patel BN, Thomas JV, Lockhart ME, Berland LL, Morgan DE. Single-source dual-energy spectral multidetector CT of pancreatic adenocarcinoma: optimization of energy level viewing significantly increases lesion contrast. *Clin Radiol* 2013;68:148-154
3. Matsumoto K, Jinzaki M, Tanami Y, Ueno A, Yamada M, Kuribayashi S. Virtual monochromatic spectral imaging with fast kilovoltage switching: improved image quality as compared with that obtained with conventional 120-kVp CT. *Radiology* 2011;259:257-262
4. Wichmann JL, Nöske EM, Kraft J, Burck I, Wagenblast J, Eckardt A, et al. Virtual monoenergetic dual-energy computed tomography: optimization of kiloelectron volt settings in head and neck cancer. *Invest Radiol* 2014;49:735-741
5. Bodanapally UK, Dreizin D, Issa G, Archer-Arroyo KL, Sudini K, Fleiter TR. Dual-energy CT in enhancing subdural effusions that masquerade as subdural hematomas: diagnosis with virtual high-monochromatic (190-keV) images. *AJNR Am J Neuroradiol* 2017;38:1946-1952
6. Bodanapally UK, Archer-Arroyo KL, Dreizin D, Shanmuganathan K, Schwartzbauer G, Li G, et al. Dual-energy computed tomography imaging of head: virtual high-energy monochromatic (190 keV) images are more reliable than standard 120 kV images for detecting traumatic intracranial hemorrhages. *J Neurotrauma* 2019;36:1375-1381
7. Zhao XM, Wang M, Wu RZ, Dharaiya E, Feng F, Li ML, et al. Dual-layer spectral detector CT monoenergetic reconstruction improves image quality of non-contrast cerebral CT as compared with conventional single energy CT. *Eur J Radiol*

2018;103:131-138
8. Pomerantz SR, Kamalian S, Zhang D, Gupta R, Rapalino O, Sahani DV, et al. Virtual monochromatic reconstruction of dual-energy unenhanced head CT at 65-75 keV maximizes image quality compared with conventional polychromatic CT. *Radiology* 2013;266:318-325
9. Forghani R, Levental M, Gupta R, Lam S, Dadfar N, Curtin HD. Different spectral hounsfield unit curve and high-energy virtual monochromatic image characteristics of squamous cell carcinoma compared with nonossified thyroid cartilage. *AJNR Am J Neuroradiol* 2015;36:1194-1200
10. Frellesen C, Kaup M, Wichmann JL, Hüsers K, Scholtz JE, Albrecht MH, et al. Noise-optimized advanced image-based virtual monoenergetic imaging for improved visualization of lung cancer: comparison with traditional virtual monoenergetic imaging. *Eur J Radiol* 2016;85:665-672
11. Sudarski S, Hagelstein C, Weis M, Schoenberg SO, Apfaltrer P. Dual-energy snap-shot perfusion CT in suspect pulmonary nodules and masses and for lung cancer staging. *Eur J Radiol* 2015;84:2393-2400
12. Weininger M, Schoepf UJ, Ramachandra A, Fink C, Rowe GW, Costello P, et al. Adenosine-stress dynamic real-time myocardial perfusion CT and adenosine-stress first-pass dual-energy myocardial perfusion CT for the assessment of acute chest pain: initial results. *Eur J Radiol* 2012;81:3703-3710
13. Arnoldi E, Lee YS, Ruzsics B, Weininger M, Spears JR, Rowley CP, et al. CT detection of myocardial blood volume deficits: dual-energy CT compared with single-energy CT spectra. *J Cardiovasc Comput Tomogr* 2011;5:421-429
14. Thieme SF, Johnson TR, Lee C, McWilliams J, Becker CR, Reiser MF, et al. Dual-energy CT for the assessment of contrast material distribution in the pulmonary parenchyma. *AJR Am J Roentgenol* 2009;193:144-149
15. Sandfort V, Palanisamy S, Symons R, Pourmorteza A, Ahlman MA, Rice K, et al. Optimized energy of spectral CT for infarct imaging: experimental validation with human validation. *J Cardiovasc Comput Tomogr* 2017;11:171-178
16. Chang S, Han K, Youn JC, Im DJ, Kim JY, Suh YJ, et al. Utility of dual-energy CT-based monochromatic imaging in the assessment of myocardial delayed enhancement in patients with cardiomyopathy. *Radiology* 2018;287:442-451
17. Lang M, Som A, Mendoza DP, Flores EJ, Reid N, Carey D, et al. Hypoxaemia related to COVID-19: vascular and perfusion abnormalities on dual-energy CT. *Lancet Infect Dis* 2020;20:1365-1366
18. Hou W, Sun X, Yin Y, Cheng J, Zhang Q, Xu J, et al. Improving image quality for lung cancer imaging with optimal monochromatic energy level in dual energy spectral computed tomography. *J Comput Assist Tomogr* 2016;40:243-247
19. Husarik DB, Gordic S, Desbiolles L, Krauss B, Leschka S, Wildermuth S, et al. Advanced virtual monoenergetic computed tomography of hyperattenuating and hypoattenuating liver lesions: ex-vivo and patient experience in various body sizes. *Invest Radiol* 2015;50:695-702
20. Marin D, Ramirez-Giraldo JC, Gupta S, Fu W, Stinnett SS, Mileto A, et al. Effect of a noise-optimized second-generation monoenergetic algorithm on image noise and conspicuity of hypervascular liver tumors: an in vitro and in vivo study. *AJR Am J Roentgenol* 2016;206:1222-1232
21. Mileto A, Nelson RC, Samei E, Choudhury KR, Jaffe TA, Wilson JM, et al. Dual-energy MDCT in hypervascular liver tumors: effect of body size on selection of the optimal monochromatic energy level. *AJR Am J Roentgenol* 2014;203:1257-1264
22. Frellesen C, Fessler F, Hardie AD, Wichmann JL, De Cecco CN, Schoepf UJ, et al. Dual-energy CT of the pancreas: improved carcinoma-to-pancreas contrast with a noise-optimized monoenergetic reconstruction algorithm. *Eur J Radiol* 2015;84:2052-2058
23. McNamara MM, Little MD, Alexander LF, Carroll LV, Beasley TM, Morgan DE. Multireader evaluation of lesion conspicuity in small pancreatic adenocarcinomas: complimentary value of iodine material density and low keV simulated monoenergetic images using multiphasic rapid kVp-switching dual energy CT. *Abdom Imaging* 2015;40:1230-1240
24. Martin SS, Wichmann JL, Pfeifer S, Leithner D, Lenga L, Reynolds MA, et al. Impact of noise-optimized virtual monoenergetic dual-energy computed tomography on image quality in patients with renal cell carcinoma. *Eur J Radiol* 2017;97:1-7
25. Martin SS, Czwikla R, Wichmann JL, Albrecht MH, Lenga L, Savage RH, et al. Dual-energy CT-based iodine quantification to differentiate abdominal malignant lymphoma from lymph node metastasis. *Eur J Radiol* 2018;105:255-260
26. Patel BN, Farjat A, Schabel C, Duvnjak P, Mileto A, Ramirez-Giraldo JC, et al. Energy-specific optimization of attenuation thresholds for low-energy virtual monoenergetic images in renal lesion evaluation. *AJR Am J Roentgenol* 2018;210:W205-W217
27. Darras KE, McLaughlin PD, Kang H, Black B, Walshe T, Chang SD, et al. Virtual monoenergetic reconstruction of contrast-enhanced dual energy CT at 70keV maximizes mural enhancement in acute small bowel obstruction. *Eur J Radiol* 2016;85:950-956
28. Lourenco PDM, Rawski R, Mohammed MF, Khosa F, Nicolaou S, McLaughlin P. Dual-energy CT iodine mapping and 40-keV monoenergetic applications in the diagnosis of acute bowel ischemia. *AJR Am J Roentgenol* 2018;211:564-570
29. Lee SM, Kim SH, Ahn SJ, Kang HJ, Kang JH, Han JK. Virtual monoenergetic dual-layer, dual-energy CT enterography: optimization of keV settings and its added value for Crohn's disease. *Eur Radiol* 2018;28:2525-2534
30. Potretzke TA, Brace CL, Lubner MG, Sampson LA, Willey BJ, Lee FT Jr. Early small-bowel ischemia: dual-energy CT improves conspicuity compared with conventional CT in a swine model. *Radiology* 2015;25:119-126
31. Murray N, Darras KE, Walstra FE, Mohammed MF, McLaughlin PD, Nicolaou S. Dual-energy CT in evaluation of the acute abdomen. *Radiographics* 2019;39:264-286

https://doi.org/10.3348/kjr.2020.0996

32. Leithner D, Mahmoudi S, Wichmann JL, Martin SS, Lenga L, Albrecht MH, et al. Evaluation of virtual monoenergetic imaging algorithms for dual-energy carotid and intracerebral CT angiography: effects on image quality, artefacts and diagnostic performance for the detection of stenosis. *Eur J Radiol* 2018;99:111-117
33. Riffel P, Haubenreisser H, Meyer M, Sudarski S, Morelli JN, Schmidt B, et al. Carotid dual-energy CT angiography: evaluation of low keV calculated monoenergetic datasets by means of a frequency-split approach for noise reduction at low keV levels. *Eur J Radiol* 2016;85:720-725
34. Neuhaus V, Abdullayev N, Große Hokamp N, Pahn G, Kabbasch C, Mpotsaris A, et al. Improvement of image quality in unenhanced dual-layer CT of the head using virtual monoenergetic images compared with polyenergetic single-energy CT. *Invest Radiol* 2017;52:470-476
35. Schneider D, Apfaltrer P, Sudarski S, Nance JW Jr, Haubenreisser H, Fink C, et al. Optimization of kiloelectron volt settings in cerebral and cervical dual-energy CT angiography determined with virtual monoenergetic imaging. *Acad Radiol* 2014;21:431-436
36. Zhang LJ, Zhao YE, Wu SY, Yeh BM, Zhou CS, Hu XB, et al. Pulmonary embolism detection with dual-energy CT: experimental study of dual-source CT in rabbits. *Radiology* 2009;252:61-70
37. Pontana F, Faivre JB, Remy-Jardin M, Flohr T, Schmidt B, Tacelli N, et al. Lung perfusion with dual-energy multidetector-row CT (MDCT): feasibility for the evaluation of acute pulmonary embolism in 117 consecutive patients. *Acad Radiol* 2008;15:1494-1504
38. Leithner D, Wichmann JL, Vogl TJ, Trommer J, Martin SS, Scholtz JE, et al. Virtual monoenergetic imaging and iodine perfusion maps improve diagnostic accuracy of dual-energy computed tomography pulmonary angiography with suboptimal contrast attenuation. *Invest Radiol* 2017;52:659-665
39. Apfaltrer P, Sudarski S, Schneider D, Nance JW Jr, Haubenreisser H, Fink C, et al. Value of monoenergetic low-kV dual energy CT datasets for improved image quality of CT pulmonary angiography. *Eur J Radiol* 2014;83:322-328
40. Sommer WH, Graser A, Becker CR, Clevert DA, Reiser MF, Nikolaou K, et al. Image quality of virtual noncontrast images derived from dual-energy CT angiography after endovascular aneurysm repair. *J Vasc Interv Radiol* 2010;21:315-321
41. Ascenti G, Mazziotti S, Lamberto S, Bottari A, Caloggero S, Racchiusa S, et al. Dual-energy CT for detection of endoleaks after endovascular abdominal aneurysm repair: usefulness of colored iodine overlay. *AJR Am J Roentgenol* 2011;196:1408-1414
42. Behrendt FF, Schmidt B, Plumhans C, Keil S, Woodruff SG, Ackermann D, et al. Image fusion in dual energy computed tomography: effect on contrast enhancement, signal-to-noise ratio and image quality in computed tomography angiography. *Invest Radiol* 2009;44:1-6
43. Karçaaltıncaba M, Aktaş A. Dual-energy CT revisited with multidetector CT: review of principles and clinical applications. *Diagn Interv Radiol* 2011;17:181-194
44. Albrecht MH, Trommer J, Wichmann JL, Scholtz JE, Martin SS, Lehnert T, et al. Comprehensive comparison of virtual monoenergetic and linearly blended reconstruction techniques in third-generation dual-source dual-energy computed tomography angiography of the thorax and abdomen. *Invest Radiol* 2016;51:582-590
45. Albrecht MH, Scholtz JE, Hüsers K, Beeres M, Bucher AM, Kaup M, et al. Advanced image-based virtual monoenergetic dual-energy CT angiography of the abdomen: optimization of kiloelectron volt settings to improve image contrast. *Eur Radiol* 2016;26:1863-1870
46. Martin SS, Wichmann JL, Scholtz JE, Leithner D, D'Angelo T, Weyer H, et al. Noise-optimized virtual monoenergetic dual-energy CT improves diagnostic accuracy for the detection of active arterial bleeding of the abdomen. *J Vasc Interv Radiol* 2017;28:1257-1266
47. Martin SS, Wichmann JL, Weyer H, Scholtz JE, Leithner D, Spandorfer A, et al. Endoleaks after endovascular aortic aneurysm repair: improved detection with noise-optimized virtual monoenergetic dual-energy CT. *Eur J Radiol* 2017;94:125-132
48. Wichmann JL, Gillott MR, De Cecco CN, Mangold S, Varga-Szemes A, Yamada R, et al. Dual-energy computed tomography angiography of the lower extremity runoff: impact of noise-optimized virtual monochromatic imaging on image quality and diagnostic accuracy. *Invest Radiol* 2016;51:139-146
49. Schabel C, Bongers M, Sedlmair M, Korn A, Grosse U, Mangold S, et al. Assessment of the hepatic veins in poor contrast conditions using dual energy CT: evaluation of a novel monoenergetic extrapolation software algorithm. *Rofo* 2014;186:591-597
50. Kulkarni NM, Sahani DV, Desai GS, Kalva SP. Indirect computed tomography venography of the lower extremities using single-source dual-energy computed tomography: advantage of low-kiloelectron volt monochromatic images. *J Vasc Interv Radiol* 2012;23:879-886
51. Weiss J, Schabel C, Othman AE, Bier G, Nikolaou K, Bamberg F, et al. Impact of dual-energy CT post-processing to differentiate venous thrombosis from iodine flux artefacts. *Eur Radiol* 2018;28:5076-5082
52. Wang CK, Tsai JM, Chuang MT, Wang MT, Huang KY, Lin RM. Bone marrow edema in vertebral compression fractures: detection with dual-energy CT. *Radiology* 2013;269:525-533
53. Tanaka R, Hayashi T, Ike M, Noto Y, Goto TK. Reduction of dark-band-like metal artifacts caused by dental implant bodies using hypothetical monoenergetic imaging after dual-energy computed tomography. *Oral Surg Oral Med Oral Pathol Oral Radiol* 2013;115:833-838
54. Bamberg F, Dierks A, Nikolaou K, Reiser MF, Becker CR, Johnson TR. Metal artifact reduction by dual energy computed tomography using monoenergetic extrapolation. *Eur Radiol*

 https://doi.org/10.3348/kjr.2020.0996

2011;21:1424-1429
55. Guggenberger R, Winklhofer S, Osterhoff G, Wanner GA, Fortunati M, Andreisek G, et al. Metallic artefact reduction with monoenergetic dual-energy CT: systematic ex vivo evaluation of posterior spinal fusion implants from various vendors and different spine levels. *Eur Radiol* 2012;22:2357-2364
56. Lewis M, Reid K, Toms AP. Reducing the effects of metal artefact using high keV monoenergetic reconstruction of dual energy CT (DECT) in hip replacements. *Skeletal Radiol* 2013;42:275-282
57. Stolzmann P, Winklhofer S, Schwendener N, Alkadhi H, Thali MJ, Ruder TD. Monoenergetic computed tomography reconstructions reduce beam hardening artifacts from dental restorations. *Forensic Sci Med Pathol* 2013;9:327-332
58. Shinohara Y, Sakamoto M, Iwata N, Kishimoto J, Kuya K, Fujii S, et al. Usefulness of monochromatic imaging with metal artifact reduction software for computed tomography angiography after intracranial aneurysm coil embolization. *Acta Radiol* 2014;55:1015-1023
59. Bongers MN, Schabel C, Thomas C, Raupach R, Notohamiprodjo M, Nikolaou K, et al. Comparison and combination of dual-energy-and iterative-based metal artefact reduction on hip prosthesis and dental implants. *PLoS One* 2015;10:e0143584
60. Komlosi P, Grady D, Smith JS, Shaffrey CI, Goode AR, Judy PG, et al. Evaluation of monoenergetic imaging to reduce metallic instrumentation artifacts in computed tomography of the cervical spine. *J Neurosurg Spine* 2015;22:34-38
61. Srinivasan A, Hoeffner E, Ibrahim M, Shah GV, LaMarca F, Mukherji SK. Utility of dual-energy CT virtual keV monochromatic series for the assessment of spinal transpedicular hardware-bone interface. *AJR Am J Roentgenol* 2013;201:878-883
62. Laukamp KR, Lennartz S, Neuhaus VF, Große Hokamp N, Rau R, Le Blanc M, et al. CT metal artifacts in patients with total hip replacements: for artifact reduction monoenergetic reconstructions and post-processing algorithms are both efficient but not similar. *Eur Radiol* 2018;28:4524-4533
63. Große Hokamp N, Neuhaus V, Abdullayev N, Laukamp K, Lennartz S, Mpotsaris A, et al. Reduction of artifacts caused by orthopedic hardware in the spine in spectral detector CT examinations using virtual monoenergetic image reconstructions and metal-artifact-reduction algorithms. *Skeletal Radiol* 2018;47:195-201
64. Henzler T, Fink C, Schoenberg SO, Schoepf UJ. Dual-energy CT: radiation dose aspects. *AJR Am J Roentgenol* 2012;199:S16-S25
65. Tawfik AM, Kerl JM, Razek AA, Bauer RW, Nour-Eldin NE, Vogl TJ, et al. Image quality and radiation dose of dual-energy CT of the head and neck compared with a standard 120-kVp acquisition. *AJNR Am J Neuroradiol* 2011;32:1994-1999
66. Shuman WP, Chan KT, Busey JM, Mitsumori LM, Koprowicz KM. Dual-energy CT aortography with 50% reduced iodine dose versus single-energy CT aortography with standard iodine dose. *Acad Radiol* 2016;23:611-618
67. Agrawal MD, Oliveira GR, Kalva SP, Pinho DF, Arellano RS, Sahani DV. Prospective comparison of reduced-iodine-dose virtual monochromatic imaging dataset from dual-energy CT angiography with standard-iodine-dose single-energy CT angiography for abdominal aortic aneurysm. *AJR Am J Roentgenol* 2016;207:W125-W132
68. Xin L, Yang X, Huang N, Du X, Zhang J, Wang Y, et al. The initial experience of the upper abdominal CT angiography using low-concentration contrast medium on dual energy spectral CT. *Abdom Imaging* 2015;40:2894-2899

https://doi.org/10.3348/kjr.2020.0996